IEEE Access
Multidisciplinary | Rapid Reviews | Open Access Journal

Received July 19, 2021, accepted July 29, 2021, date of publication August 2, 2021, date of current version August 9, 2021.

Digital Object Identifier 10.1109/ACCESS.2021.3101942

Improved Three-Phase Integrated Charger Converter Connected to Single-Phase Grid With Torque Cancellation

JAIME PANDO-ACEDO[1], MARÍA ISABEL MILANÉS-MONTERO[1], ENRIQUE ROMERO-CADAVAL[1], (Senior Member, IEEE), FERNANDO BRIZ[2], (Senior Member, IEEE), AND FERMÍN BARRERO-GONZÁLEZ[1], (Senior Member, IEEE)

[1]Department of Electric, Electronic and Automation Engineering, University of Extremadura, 06006 Badajoz, Spain
[2]Department of Electrical, Electronics, Computers and Systems Engineering, University of Oviedo, 33204 Gijón, Spain

Corresponding author: Fermín Barrero-González (fbarrero@unex.es)

This work was supported in part by the Government of Extremadura through the Predoctoral Training Program under Grant PD16044, and in part by the Funding for Research Groups under Grant GR18087.

ABSTRACT Although there is a growing interest in developing fast charging methods to enhance the Electric Vehicles' appeal, the main energy supply is still the single-phase outlet. While single-phase charging may be simpler than three-phase, there are challenges in the integration of the propulsion and charging systems without adding inductive grid filters. Such integration would bring benefits like the simplification and reduction of components, costs, volume or weight. This can be achieved by using the windings of the propulsion machine as grid filters, but the use of the electric motor as a grid inductive filter leads to the generation of pulsating torque during the charging state. This translates into vibration, noise and eventually, damage to the motor and other components of the system. In this work, the authors propose a control strategy that considerably reduces the peaks of pulsating torque generated in any rotor position while using the machine wingdings as filter. Simulation tests have been carried out to validate the control strategy, taking into account the system efficiency. Finally, experiments are conducted to prove that the reduction of the torque pulsation is achieved.

INDEX TERMS Integrated charger, electric vehicles (EV), permanent magnet synchronous motor (PMSM), battery charger.

I. INTRODUCTION

The Electric Vehicle (EV) is gaining popularity due to environmental concerns and motivates research related to it. Special interest is put into the charging process, since the energy stored in the EV battery can also be used for grid services [1]. The charger topologies also receives a fair amount of attention, since it is desirable to charge the EV with the higher efficiency and as fast as possible [2].

According to the charging power level, chargers can be roughly classified into Level 1 (up to 1.92 kW), Level 2 (up to 19.2 kW) and Level 3 (from 20 kW onwards) [3], [4]. The higher the charging power, the more complex the charger will be, needing more components or bigger ones. Therefore, Level 3 chargers are located off-board while the other two are usually located on-board. Although three phase connections to the grid allows faster charging, single phase outlets are still the main source of energy available to EV owners [5].

Due to the fact that the propulsion and charging systems share quite a few elements, there is a trend of integrating the charging system into the power electronics already present for driving the motor [6]–[8]. In this case, the onboard charger becomes an Integrated Onboard Charger (IOC). The propulsion inverter can be easily adapted for the charging process, and the motor windings could be employed as inductive filters.

Some authors propose to use additional rectifiers for the AC/DC conversion from the grid, then the machine windings as inductors for a DC/DC converter [9]–[11]. The main drawback is the need of additional components that will translate

The associate editor coordinating the review of this manuscript and approving it for publication was Kan Liu.

into an increment of the cost, losses, volume and weight. In other cases, as in this work, the machine windings is used as a grid filter connected between the grid and the converter, which is used later on for AC/DC conversion [12]–[16]. The principal disadvantage is the generation of a charging torque in the shaft due to the grid currents flowing through the machine.

The cancellation of the torque generated on the machine has been receiving quite a lot of attention lately. The torque generated is analyzed in [17] and the authors propose to use a brake to mitigate it, which causes extra noise and increments the cost of the system. Other solutions proposed include using several machines [14], custom windings [12] and multiphase machines [10], [13], [18], [19]. These innovative solutions require said special components that are still not present in the wide majority of EV systems. Moreover, the torque cancellation strategy in single phase chargers normally assumes that the phase connected to the grid is aligned with rotor d-axis, where no torque is produced [8], [10], [19]. This provokes a lack of generality, since it is vital to have an optimized control strategy that guarantees the absence of vibrations in the system. In this paper, a torque cancellation strategy is presented for a single-phase charger that uses the windings of a three-phase Permanent Magnet Synchronous Motor (PMSM) as a grid filter. Moreover, there is no need of having the neutral or middle points of the windings available. Such a charger is able to operate reducing the vibrations, no matter the position of the rotor while charging, therefore extending the lifetime of the motor and components attached to it.

The paper is structured as follows. First, an overview of the problem and an analysis of the torque generated during the charging operation is presented. Afterwards, the strategy proposed for the torque removal will be discussed and simulation results will be provided. Lastly, experimental results will validate the successful operation of the control developed.

II. PROBLEM DESCRIPTION

Having currents circulating in the machine windings will give raise to magnetic fields in the airgap. These fields will interact with the field established by the magnets in the rotor, for the case of a PMSM. This interaction will lead to the appearance of torque in the machine's shaft. The nature of this torque will depend mainly on the grid's frequency as well as the connection of the machine windings. In this section, the currents and torque produced will be analysed properly, and the strategy to cancel the torque produced will be presented.

A. ANALYSIS OF THE TORQUE OSCILLATIONS

Figure 1 shows a conventional topology for single phase onboard charger connection. It is made up of the propulsion machine, a three phase inverter and two commutators that will change their position according to the operation mode. In the propulsion mode, represented in Figure 1a), the two commutators will remain in the *OFF* mode, and the three phases of the motor will be connected to the inverter midpoints A,B,C.

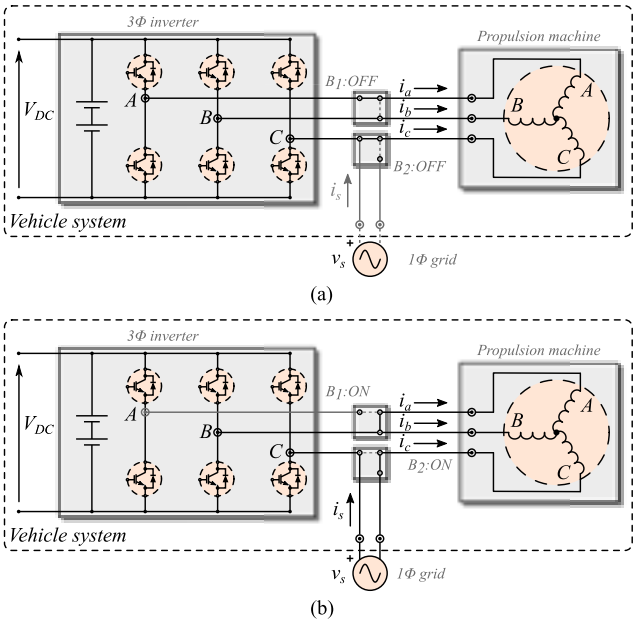

FIGURE 1. Vehicle system connected to a single phase grid. a) Propulsion mode b) Charging mode.

In this case, the phase currents i_a, i_b, i_c will be determined by the controller in order to drive the motor accordingly. When the system is in charging mode, the commutators switch to *ON*, and the overall scheme is the one depicted in the Figure 1b). In this case, the current demanded to the grid i_s will be equal in magnitude to one of the phases current but with a 180 degrees shift. In this example, the grid current will be i_c but shifted. Thus, if it is assumed that the motor windings are identical in each phase, one can write

$$\begin{aligned} i_c &= -i_s \\ i_a &= i_b = -\frac{i_c}{2}. \end{aligned} \tag{1}$$

The current demanded form the grid can be ideally described by the following expression

$$i_s = \sqrt{2} I_s \cos(\omega t), \tag{2}$$

where ω is the angular frequency, t is the time variable and I_S is the RMS value. The phase currents in the machine can be expressed in field coordinates as

$$\begin{bmatrix} i_d \\ i_q \\ i_0 \end{bmatrix} = \frac{2}{3} [K] \begin{bmatrix} i_a \\ i_b \\ i_c \end{bmatrix}, \tag{3}$$

where K is the transformation matrix for the $dq0$ transform, and is given by

$$[K] = \begin{bmatrix} \cos(\theta) & \cos(\theta - \frac{2\pi}{3}) & \cos(\theta + \frac{2\pi}{3}) \\ -\sin(\theta) & -\sin(\theta - \frac{2\pi}{3}) & -\sin(\theta + \frac{2\pi}{3}) \\ \frac{1}{2} & \frac{1}{2} & \frac{1}{2} \end{bmatrix}, \tag{4}$$

TABLE 1. Parameters of the PMSM.

Symbol	Quantity	Value
V_n	Nominal voltage	230 V
I_n	Nominal current	22 A
T_n	Nominal torque	31, 18 Nm
R_s	Stator resistance	0.7 Ω
L_d	Direct axis inductance	1.616×10^{-3} H
L_q	Quadrature axis inductance	1.871×10^{-3} H
J	Inertia	3.6×10^{-3} Kgm^2
p	Pole pairs	4
λ	Magnet flux linkage	0.1323 Vs

where θ is the angle between the d and the a axis. Using (1) and (4), the direct and quadrature currents in (3) can be expressed as

$$i_d = -i_s \cos\left(\theta + \frac{2\pi}{3}\right)$$
$$i_q = i_s \sin\left(\theta + \frac{2\pi}{3}\right). \quad (5)$$

Note that the 0 component has been omitted since a three-wire system is being considered. For the case of a PMSM, the torque produced in the machine can be expressed as a function of the d and q-axis currents as

$$T_e = \frac{3}{2} p \left(L_d - L_q\right) i_d i_q + \lambda i_q, \quad (6)$$

where L_d, L_q are the direct and quadrature inductances of the machine, p are the pole pairs, and λ is the magnet flux linkage. Substituting (5) into (6), and taking into account the expression for the grid current (2), the torque developed by the machine during the charging state can be described by

$$T_e = -\frac{3}{4} p L_\Delta I_s^2 \left(1 + \cos(2\omega t)\right) \sin\left(2\theta + \frac{4\pi}{3}\right) + \lambda\sqrt{2} I_s \cos(\omega t) \sin\left(\theta + \frac{2\pi}{3}\right). \quad (7)$$

where $L_\Delta = L_d - L_q$. From (7) it can be observed that the torque will have three main components: a DC component, a component located at the grid frequency and the last one at twice the grid frequency. Depending on the characteristics of the motor, the first term of (7), which is the one holding the DC and the 2ω components, will be noticeable or not. To be more precise, said components will be present in Interior mounted PMSM (IPMSM), but not in Surface mounted PMSM (SPMSM). This fact can be observed in Figure 2, where the frequency analysis of the simulation results for the torque produced in the machine during the charging state are presented. The components are located at 0, 50 and 100 Hz since the grid frequency is 50 Hz. The three amplitudes of the three components mentioned are represented for different rotor positions. This simulation uses the machine parameters presented in Table 1, but for the case of Figure 2(a), L_q is modified so the salience factor is 5, i.e., $L_q/L_d = 5$. This is typically the case for IPMSM, whereas unity salience factors can be found in SPMSM. In this simulation, the value of I_s is fixed at 16 A, with unity power factor, and the converter is simulated as an ideal current source.

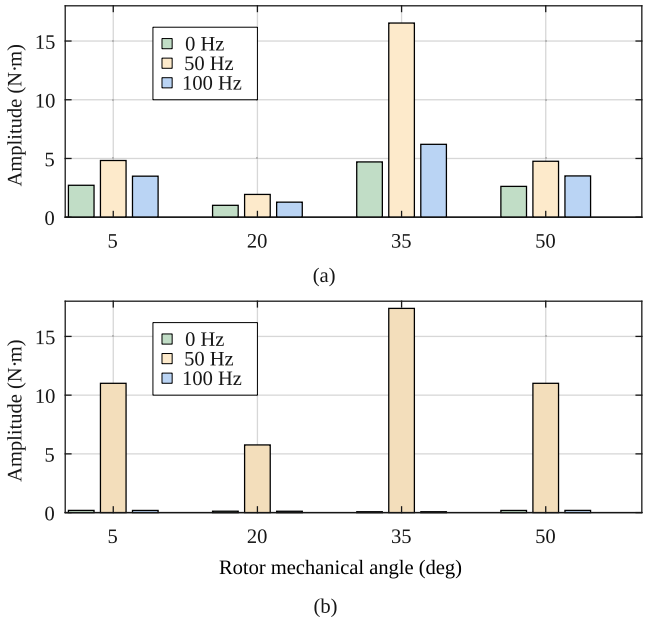

FIGURE 2. Torque components developed by the machine when the system is operating in charging mode with a grid frequency of 50 Hz, for different rotor positions. (a) Interior mounted PMSM. (b) Surface mounted PMSM.

It can also be noted in both cases represented in Figure 2 how the torque oscillations amplitude depends on the rotor angle. The angles selected for the figure sweep across different points of operation where minimum and maximum torque is generated. This can be confirmed in (7), where the minimum and maximum values for the torque will be reached when

$$T_{min} \Rightarrow \theta = \left\{\frac{\pi}{3}, \frac{4\pi}{3}\right\} rad,$$
$$T_{max} \Rightarrow \theta = \left\{\frac{5\pi}{6}, \frac{11\pi}{6}\right\} rad. \quad (8)$$

Note that the angles stated in (8) are referred to (7), and therefore are electrical radians. The relationship between electrical and mechanical angles is given by $\theta = p \cdot \alpha$, where α is the mechanical angle. As a reference, the first minimum and maximum angle rotors in (8) would translate to 15 and 37.5 mechanical degrees, given the machine pole pairs. This can be confirmed with the results shown in Figure 2.

In the case that the grid is connected to another of the two remaining phases, similar results are to be expected, at rotor angles shifted by $2\pi/3$ rad. Nevertheless, this oscillations represent a hazard for the system and should be eliminated. In the literature consulted, this problem has yet to be addressed or it is assumed that one can select the most favorable position for the rotor prior to the charging state. However, this could not be the case or it would need extra components like a clutch in order to be able to allow the rotor to turn without moving the vehicle. Therefore, there is a need to come up with a solution that allow to charge the EV no matter the rotor angle. This will be addressed in the next section.

B. TORQUE OSCILLATIONS REMOVAL

One can note that, by setting the commutator $B_1 = ON$ in Figure 1(a), one degree of freedom of the current system is lost. This is represented by (1), where one current of the system is set and the other two vary accordingly.

Now, let us consider that the commutator B_1 is set to OFF, while keeping $B_2 = ON$,i.e., in charging state. In that case, one can set two of the three system currents. If we also control the current i_b, the third current will be set by the other two following

$$i_a^* = -\left(i_b + i_c\right), \tag{9}$$

since we are already controlling the i_c current as

$$i_c^* = -i_s = -\sqrt{2} I_s \cos \omega t. \tag{10}$$

In order to be able to cancel the torque oscillations, recalling (6), it would suffice to cancel out current i_q. Using the definition introduced in (4) one could write

$$i_q = \frac{2}{3}\Bigg[- i_a \sin(\theta) - i_b \sin\left(\theta - \frac{2\pi}{3}\right) - i_c \sin\left(\theta + \frac{2\pi}{3}\right)\Bigg] \tag{11}$$

By using the two degrees of freedom aforementioned in (9), and forcing $i_q = 0$ in (11), the expression for the current i_b is given by

$$i_b^* = i_c^* \left[\frac{\sin(\theta) - \sin\left(\theta + \frac{2\pi}{3}\right)}{\sin\left(\theta - \frac{2\pi}{3}\right) - \sin(\theta)}\right]. \tag{12}$$

Ideally, forcing i_b to follow (12) would cancel i_q and eliminate any torque oscillation. However, note that this expression depends on the rotor angle θ and therefore, values that cancel the denominator could make the current demanded in phase B infinite. This can be observed in Figure 3(a), where the RMS values of the three phases requires to cancel the q-axis current are represented for a complete electrical revolution of the rotor. The RMS value in phase C is constant and fixed at 16 A for this example, while the values for phases A and B vary accordingly. Note that, for rotor angles where the torque is maximum as in (8), phases A and B ramp up to impossible values. Therefore, some restrictions must be applied for the reference currents.

Since our main goals is to minimize the torque oscillations without exceeding the nominal currents, no matter the rotor position, all the currents must be scaled down at the same time, so the condition of $i_q = 0$ is always met. In order to scale down the currents, a scaling factor is introduced as

$$s = \begin{cases} 1 & 0 < I_{RMS\_max} < I_n \\ \dfrac{I_n}{I_{RMS\_max}} & I_n \leq I_{RMS\_max} \end{cases} \tag{13}$$

where $I_{RMS\_max} = \max(I_a, I_b, I_c)$, and I_n is the nominal current of the machine. This scaling factor as a function of the rotor position is depicted in Figure 3(b). Then, the reference currents used to drive the inverter can be simply expressed as

$$i_{abc}^{*SC} = s \cdot i_{abc}, \tag{14}$$

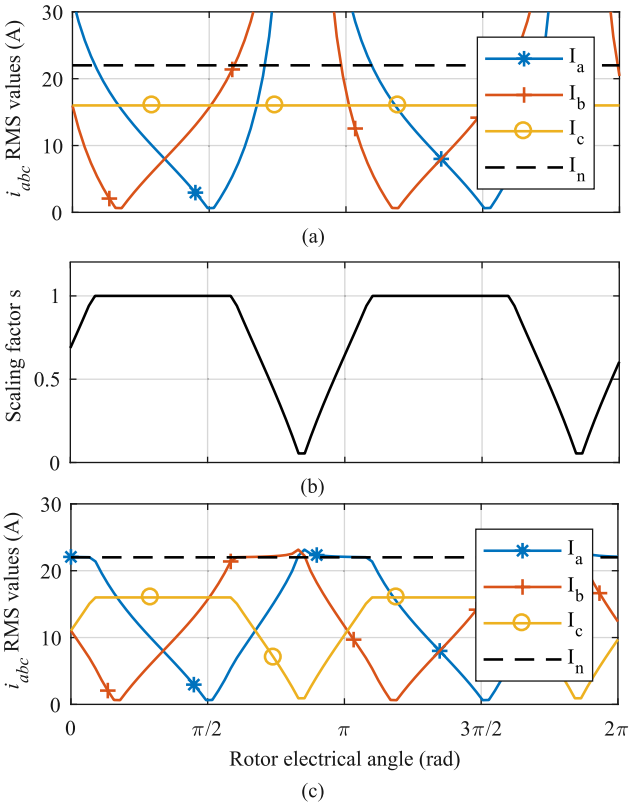

FIGURE 3. Scaling operation of the torque cancellation technique. (a) RMS values of the phase currents prior to scaling. (b) Scaling factor applied. (c) RMS values of the phase currents after scaling.

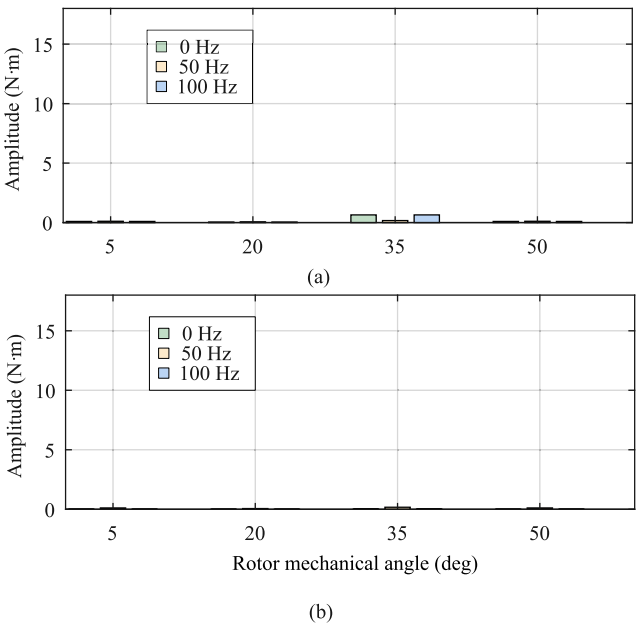

FIGURE 4. Torque components developed by the machine when the system is operating in charging mode and $i_q = 0$. (a) Interior mounted PMSM. (b) Surface mounted PMSM.

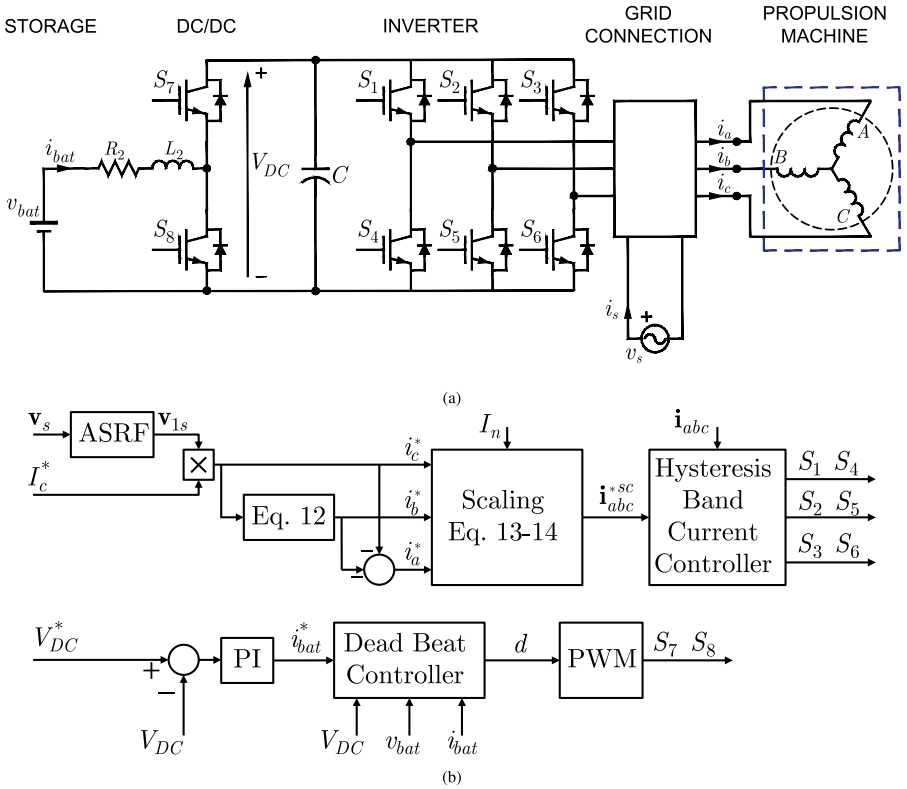

FIGURE 5. Simulation and experiment power and control setup. (a) Power topology of the system including storage, DC/DC converter, inverter, grid connection and propulsion machine. (b) Control block diagram for the whole system.

which are shown in Figure 3(c). When the rotor position is near the values for maximum torque, all the currents are scaled down so the rated current is not overcomed. Using the scaling discussed, the same simulation performed in the previous section is carried out, and its results are presented in Figure 4. Compared to Figure 2, the amplitude of the main torque components is close to zero for all rotor positions, including the ones near the angles where the maximum torque is produced. Although the torque components are dramatically reduced, note that from Figure 3(c) it can be seen that the current in phase C, which is the one demanded from the grid and used to charge the vehicle can be severely reduced using this technique, which will heavily impact the charging power and thus, the charging speed. Therefore, no matter if one can reduce the torque produced by the charging process if the charging itself is compromised. It is imperative to find a solution that allows a good charging efficiency while reducing the torque produced.

III. SIMULATION RESULTS

In order to study the charging efficiency deeply, a more complete simulation is conducted. The complete power topology under study for the simulation and experimental results is the one depicted in Figure 5 (a). A three phase IGBT inverter with hysteresis current regulator is used, and the DC bus voltage is regulated using an extra IGBT branch to boost up the voltage

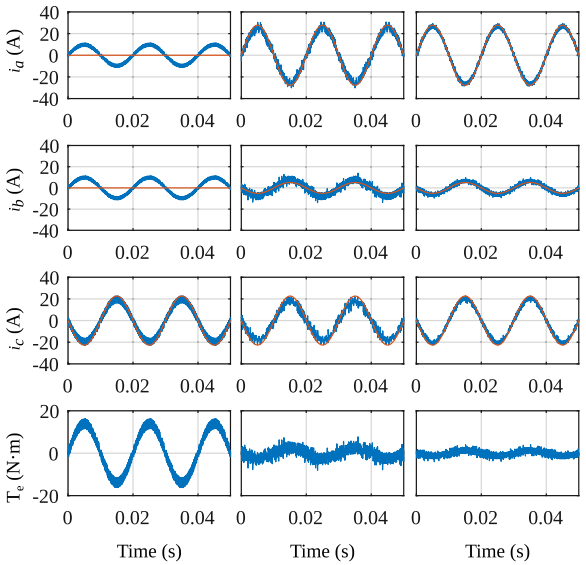

FIGURE 6. Simulation results comparing the parallel topology (left column) versus the proposed one (center and right column), for a rotor electrical angle $\theta = 20$ deg. The reference currents are represented by a dashed red line, while the currents flowing through the machine are depicted in solid blue, as the electromagnetic torque. The commutation frequency in the left and center column is 10 kHz, and 20 kHz for the right one.

coming from a battery. The control diagram of the whole system is the one showed in Figure 5 (b). An Asynchronous Reference Frame (ASRF) [20] is used to synchronize the

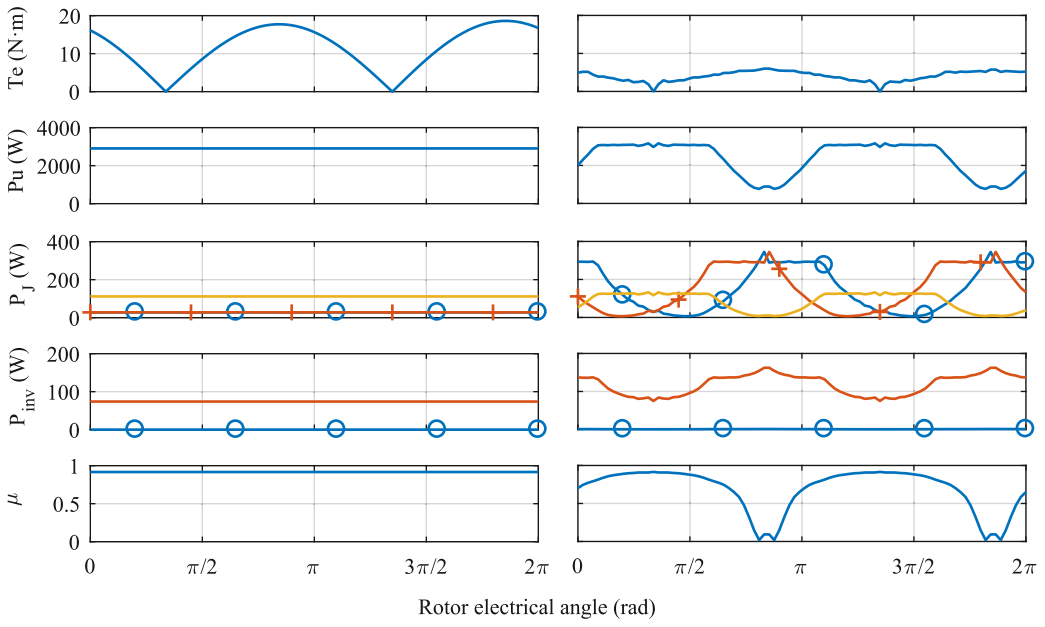

FIGURE 7. Simulation results comparing the parallel topology (left) with the proposed one (right), for a complete rotor electrical revolution. From top to bottom: torque developed by the machine; power demanded by the grid; machine losses for phase A (blue line with circle markers), phase B (orange line with cross markers) and phase C (solid yellow line); inverter switching losses (blue line with circle markers) and conduction losses (orange solid line); charging efficiency.

TABLE 2. Parameters of the simulation.

Symbol	Quantity	Value
T_f	Simulation time step	10^{-6} s
T_s	Sampling time	5^{-5} s
D_v	Diode voltage drop	1.8 V
SW_v	Switch voltage drop	3.7 V
SW_{ON}	Switch ON energy	10.5×10^{-3} J
SW_{OFF}	Switch OFF energy	7.5×10^{-3} J
D_e	Diode recuperation energy	3×10^{-3} J
D_{OFF}	Diode resistance	32×10^{-3} Ω
SW_r	Switch resistance	76×10^{-3} Ω

grid current with the phase voltage and achieve unity PF. The DC/DC converter uses a Proportional-Integral and Dead Beat controllers to ensure the DC bus voltage follows the reference. PWM is then used to generate the switching signals for the converter. The main parameters of the simulation and the semiconductors used are shown in Table 2.

The first test consists in demanding the maximum current allowed in home appliances, i.e., $I_C = 16$A, for a fixed rotor electrical angle $\theta = 20$ deg. It will compare the torque produced by the parallel charging topology represented by Figure 1b) with the one proposed. The results are shown in Figure 6. It can be seen that, although the torque is greatly reduced, torque pulsations are not completely eliminated as it was the case in the ideal case, represented by Figure 4. This is due to the limited performance of the hysteresis band to follow the references. Higher commutation frequencies could improve the results, as the right column in Figure 6 shows, where the frequency is rised from 10 kHz to 20 kHz. However, they are kept at 10 kHz in order to better compare to the experimental results that will be presented in next section.

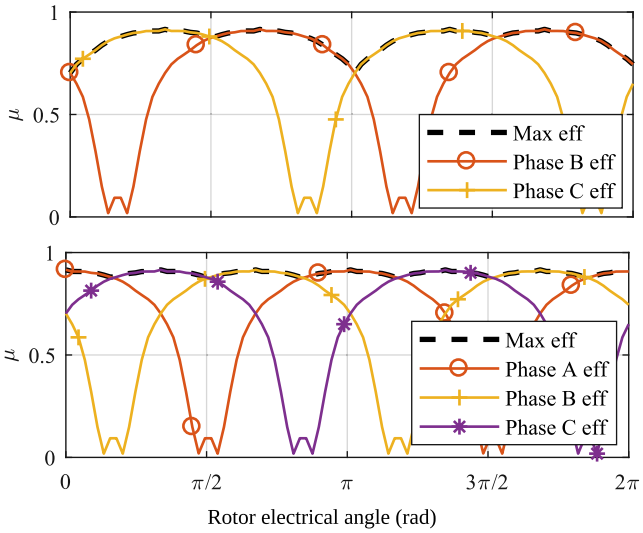

FIGURE 8. Simulation results showing the efficiency of each branch and the maximum combined efficiency achieved. The top plot shows the efficiency combined when using two branches and the bottom one, when using three branches.

As it was stated in the previous section, one drawback of scaling the currents as in (14) is that the charging speed is severely affected, depending on the rotor position. This situation is depicted in Figure 7, where the simulations for a complete electrical revolution of the rotor is presented. The figure presents another comparative of the two topologies, maintaining constant the current reference of phase C (the one connected to the grid) for the parallel topology, but enabling the scaling if needed for the case of the proposed strategy. The torque is greatly reduced in any position, but the effective

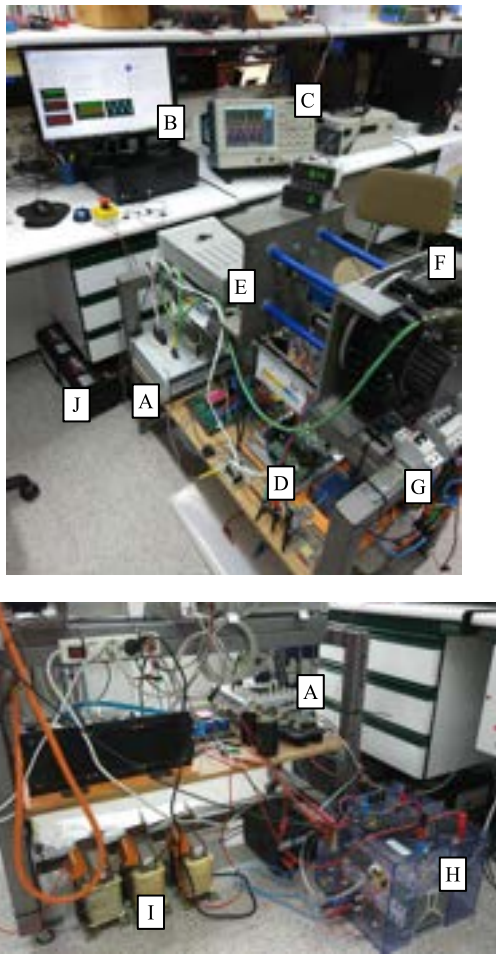

FIGURE 9. Experimental testbench for the conducted experiments. A: dSPACE control platform. B: ControlDesk software. C: Oscilloscope. D: Three-phase inverter. E: Magnetic dust brake. F: PMSM. G: Single-phase grid connection. H: DC/DC converter. I: DC inductive filter. J: 96 V battery storage.

power demanded from the grid, P_u, is reduced considerably at the maximum torque positions. Moreover, in this case, also the inverter loses along with the machine losses are considered. Thus, the power and losses terms are defined as

$$\begin{aligned} P_u &= V_s I_s \\ P_J &= (I_{abc})^2 R_s \\ P_{inv} &= P_{SW} + P_{ON} \end{aligned} \tag{15}$$

where P_{SW} and P_{ON} are the switching and conduction losses of the three branch inverter, and are calculated according to [21]. Taking (15), the efficiency is calculated as

$$\mu = 1 - \frac{P_J + P_{inv}}{P_u} \tag{16}$$

It can be observed that for the angles where the maximum torque is produced, the efficiency has margin for improvement. As it was stated previously, it is imperative that the system has to be able to charge no matter the rotor angle, while achieving torque cancellation. However, if the voltage source is connected in any of the other two phases,

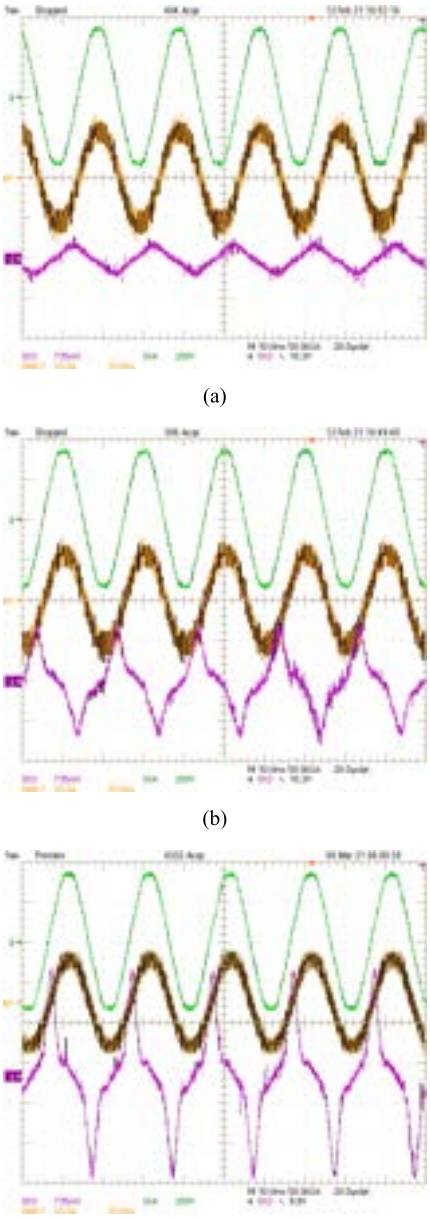

(a)

(b)

(c)

FIGURE 10. Experiments results for the parallel topology. Three different rotor positions: (a) $\theta = 1.02$ rad, (b) $\theta = 1.4$ rad, (c) $\theta = 2.6$ rad. From top to bottom: grid voltage v_s (200 V/div), grid current i_s (20 A/div) and torque (10 Nm/div).

the efficiency curve is shifted $2\pi/3$ electrical radians. In this way, the points of minimum efficiency can be avoided while retaining the advantage of reducing the torque generated by the machine. The efficiency could be further improved by allowing the connection to the single phase grid in any of the three branches, which would allow an efficiency curve almost flat and equal to the parallel topology. This situation is illustrated in Figure 8, for a complete electrical revolution of the rotor. The efficiency ranges from $[0.70, 0.91]$ for the case that the grid is connected to the best out of two phases (C or B) and needing only one commutator, and from $[0.88, 0.91]$ for the case that the grid is connected to

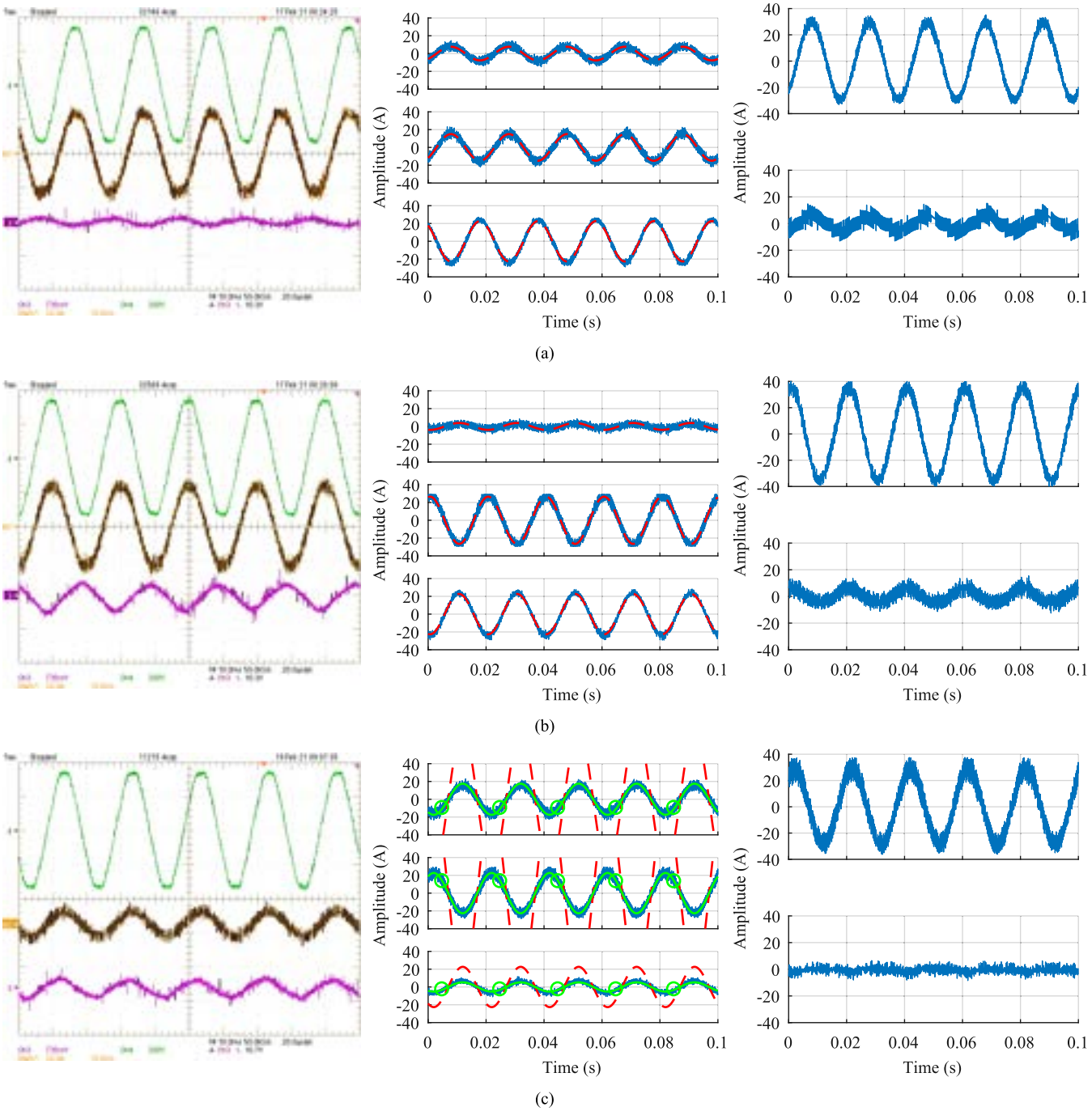

FIGURE 11. Experiment results using the three phase topology, with the torque cancellation strategy. Three rotor positions: (a) $\theta = 1.02$ rad, (b) $\theta = 1.4$ rad, (c) $\theta = 2.6$ rad. The left column are the oscilloscope captures showing the grid voltage v_s (200 V/div), grid current i_s (20 A/div) and torque (10 Nm/div), from top to bottom. The middle column show the motor currents i_{abc} as measured by the control platform (reference current as a dashed red line, scaled reference in green with circle markers and measured current in solid blue). The right column show the motor currents in the *dq*0 reference frame (d current top, q current bottom).

the most favorable phase voltage, needing two additional commutators.

Therefore, to ensure that the electric vehicle is charging at the highest possible efficiency, the phase of the grid to be connected to the charger is determined according to the known rotor position. In this way, according to Figure 8 bottom, for the case of using three branches, phase A will be selected if rotor angle is between 0 to $\pi/6$ or between $5\pi/6$ and π; phase C if the rotor angle is between $\pi/6$ and $\pi/2$, and phase B if it is between $\pi/2$ and $5\pi/6$. The election is similar for the other half cycle (from π to 2π). With this method, efficiency will be at least 88 %. Another method, that will not need to measure or estimate the rotor position, would be to try sequentially the three phases at the moment of

TABLE 3. Experimental results comparing the parallel topology (2ϕ) with the proposed one (3ϕ). The THD is computed on the current of the phase connected to the grid, μ is the charger efficiency and the torque factor is given by $\Delta T = T_{pp}/T_n$.

	THD_{i_s}		μ		ΔT	
θ (rad)	2ϕ	3ϕ	2ϕ	3ϕ	2ϕ	3ϕ
1.02	17.16%	13.74%	0.89	0.86	0.25	0.06
1.4	17.82%	13.49%	0.88	0.84	0.83	0.32
2.6	16.75%	41.61%	0.90	0.347	1.66	0.19

connection and selecting the one that produces the highest efficiency.

IV. EXPERIMENTAL RESULTS

In order to test the performance of the strategy proposed, experimental tests are conducted. The two topologies discussed and represented in Figure 1 are implemented on a testbench using a surface mounted PMSM which has the same parameters used during the simulations, i.e., the ones showed in Table 1. The system uses an IGBT inverter controlled by a dSPACE platform, employing hysteresis band current control as it was done in simulation. The software ControlDesk is used for controlling the dSPACE platform and for recording some of the experimental data. The testbench is showed in Figure 9. In both cases, the grid is connected to phase C of the machine, as it has been analysed during the whole paper.

The first test results, representing the parallel topology, is depicted in Figure 10. Three different rotor positions are represented, and for each one the grid voltage v_s, current i_s and torque measured in the shaft of the machine. In the three experiments conducted, the grid current RMS value is fixed at 16 A since it is an usual value for domestic consumers. This current is kept in phase with the grid voltage in order to achieve unity power factor. It can be observed that, the closer one gets to angle values of maximum torque, torque peaks around 20 Nm can be observed. This would severely affect mechanical elements connected to the shaft of the machine.

Next, the same experiments are conducted using the strategy proposed, and its results presented in Figure 11, where each row corresponds to a different rotor position. The current level for i_s is kept at 16 A, and the reference currents i_a^*, i_b^* and i_c^* are calculated according to (9), (10) and (12) respectively. The left column of the figure shows the oscilloscope captures showing the same information as Figure 10, where it can be seen that the currents are kept in phase with the grid voltage as before. In the third row, it can be seen that the current magnitude for the grid current is much smaller than in the other two cases. This is because in this rotor position, the other two currents needed for torque cancellation are so high that require scaling, and so does the grid current. In any case, it can be seen how the torque peaks are severely reduced. However, there is still some torque developed as discussed for in the simulations results depicted in Figure 7, the main reason being the hysteresis current controller. In the second column one can see the reference currents in the *abc* reference frame, the scaled references when scaling is used, and the phase currents measured by the control platform. Again, for the third rotor position, the reference currents exceed the maximum currents allowed, and thus they are scaled down in order to guarantee that the nominal currents are not overcomed and still generate the minimum torque possible in the rotor shaft. Lastly, the measured currents in the *dq* reference frame are depicted in the right column. Here it can be seen that there is still some current in the q axis, again due to the current controller performance. It is worth noting that the strategy proposed can be implemented with any other current controller, so there is no lack of generality.

The results of the comparison are also summarized in Table 3. The table shows the THD for the grid current, the efficiency of the charger and the torque observed as a factor given by $\Delta T = T_{pp}/T_n$, where T_{pp} is the peak to peak torque and T_n is the nominal torque from Table 1. The THD for the grid current i_s shows better results for the proposed topology, except for the scaling scenario, since the fundamental component of the current is reduced considerably. The efficiency is in good agreement with the simulation results from Figure 7. It can be seen that in the two first rotor positions there is almost no reduction in efficiency. For the third case, the scaling reduces the charging current and the efficiency drops. However, the torque factor also drops from 1.66 to 0.19 (a 88 % reduction). In any case, if the phase connected to the grid is switched for the last rotor position, the heavy scaling can be avoided retaining the high efficiency and torque reduction.

V. CONCLUSION

The use of the machine windings as grid inductors in single-phase IOC of EVs give raise to torque pulsations in the shaft. In this paper, this torque is analyzed for a EV propelled by a three-phase PMSM. It is found that, by controlling not only the grid current but the three currents flowing through the machine windings, the torque can be cancelled in any rotor position.

The proposed control strategy only needs the power electronics already present for the propulsion system of the EV plus one or two commutators to achieve the maximum efficiency. By commutating the connection to the grid between 2 or more phases, the charging performance of the system can be optimized.

When the torque cancelling currents overpass the nominal currents of the motor, they are scaled down to guarantee the safe operation of the machine. Simulation results prove the correct operation and efficiency of the system, and experiments are conducted to confirm it. Although the current controller's performance is not ideal, an 88% torque reduction is achieved in the worst case scenario.

REFERENCES

[1] V. Monteiro, J. G. Pinto, and J. L. Afonso, "Operation modes for the electric vehicle in smart grids and smart homes: Present and proposed modes," *IEEE Trans. Veh. Technol.*, vol. 65, no. 3, pp. 1007–1020, Mar. 2016.
[2] A. Khaligh and M. D'Antonio, "Global trends in high-power on-board chargers for electric vehicles," *IEEE Trans. Veh. Technol.*, vol. 68, no. 4, pp. 3306–3324, Apr. 2019.
[3] M. Yilmaz and P. T. Krein, "Review of battery charger topologies, charging power levels, and infrastructure for plug-in electric and hybrid vehicles," *IEEE Trans. Power Electron.*, vol. 28, no. 5, pp. 2151–2169, May 2013.

[4] S. Rivera, S. Kouro, S. Vazquez, S. M. Goetz, R. Lizana, and E. Romero-Cadaval, "Electric vehicle charging infrastructure–from grid to battery," *IEEE Ind. Electron. Mag.*, vol. 15, no. 2, pp. 37–51, Jun. 2021.
[5] I. Subotic and E. Levi, "A review of single-phase on-board integrated battery charging topologies for electric vehicles," in *Proc. IEEE Workshop Elect. Mach. Design, Control Diagnosis (WEMDCD)*, Mar. 2015, pp. 136–145.
[6] D.-H. Kim, M.-J. Kim, and B.-K. Lee, "An integrated battery charger with high power density and efficiency for electric vehicles," *IEEE Trans. Power Electron.*, vol. 32, no. 6, pp. 4553–4565, Jun. 2017.
[7] C. Shi and A. Khaligh, "A two-stage three-phase integrated charger for electric vehicles with dual cascaded control strategy," *IEEE J. Emerg. Sel. Topics Power Electron.*, vol. 6, no. 2, pp. 898–909, Jun. 2018.
[8] J. Ye, C. Shi, and A. Khaligh, "Single-phase charging operation of a three-phase integrated onboard charger for electric vehicles," in *Proc. IEEE Trans. Transport. Electrific. Conf. Expo (ITEC)*, Jun. 2018, pp. 681–686.
[9] V. F. Pires, A. Cordeiro, D. Foito, and J. F. Silva, "A three-phase on-board integrated battery charger for EVs with six-phase machine and nine switch converter," in *Proc. IEEE 13th Int. Conf. Compat., Power Electron. Power Eng. (CPE-POWERENG)*, Apr. 2019, pp. 1–6.
[10] Y. Xiao, C. Liu, and F. Yu, "An effective charging-torque elimination method for six-phase integrated on-board EV chargers," *IEEE Trans. Power Electron.*, vol. 35, no. 3, pp. 2776–2786, Mar. 2020.
[11] C. Shi, Y. Tang, and A. Khaligh, "A single-phase integrated onboard battery charger using propulsion system for plug-in electric vehicles," *IEEE Trans. Veh. Technol.*, vol. 66, no. 12, pp. 10899–10910, Dec. 2017.
[12] J. Gao, D. Jiang, W. Sun, and Y. Zhang, "Zero torque three phase integrated on-board charger by multi-elements motor torque cancellation," in *Proc. IEEE Energy Convers. Congr. Expo. (ECCE)*, Sep. 2019, pp. 563–568.
[13] S. Q. Ali, D. Mascarella, G. Joos, and L. Tan, "Torque cancelation of integrated battery charger based on six-phase permanent magnet synchronous motor drives for electric vehicles," *IEEE Trans. Transport. Electrific.*, vol. 4, no. 2, pp. 344–354, Jun. 2018.
[14] S. Q. Ali, D. Mascarella, G. Joos, and L. Tan, "Torque elimination for integrated battery charger based on two permanent magnet synchronous motor drives for electric vehicles," *IET Electr. Power Appl.*, vol. 11, no. 9, pp. 1627–1635, Nov. 2017. [Online]. Available: https://ietresearch.onlinelibrary.wiley.com/doi/pdf/10.1049/iet-epa.2017.030%2
[15] S. Sharma, M. V. Aware, and A. Bhowate, "Integrated battery charger for EV by using three-phase induction motor stator windings as filter," *IEEE Trans. Transport. Electrific.*, vol. 6, no. 1, pp. 83–94, Mar. 2020.
[16] S. He, Z. Xu, M. Chen, H. Yang, and W. Li, "General derivation law with torque-free achieving of integral on-board charger on compact powertrains," *IEEE Trans. Ind. Electron.*, vol. 68, no. 2, pp. 1791–1802, Feb. 2021.
[17] D. Zhuolin, Z. Feng, C. Wei, W. Yongxing, Z. Dong, and W. Xuhui, "Analysis of charging torque in a three-phase integrated charger of electrical vehicle," in *Proc. IEEE Conf. Expo Transp. Electrific. Asia–Pacific (ITEC Asia–Pacific)*, Aug. 2014, pp. 1–5.
[18] I. Subotic, N. Bodo, and E. Levi, "An EV drive-train with integrated fast charging capability," *IEEE Trans. Power Electron.*, vol. 31, no. 2, pp. 1461–1471, Feb. 2016.
[19] J. Gao, W. Sun, D. Jiang, Y. Zhang, and R. Qu, "Improved operation and control of single-phase integrated on-board charger system," *IEEE Trans. Power Electron.*, vol. 36, no. 4, pp. 4752–4765, Apr. 2021.
[20] M. I. M. Montero, E. R. Cadaval, and F. B. Gonzalez, "A novel fundamental voltage synchronization control strategy for shunt single-phase and three-phase active power filters," in *Proc. IEEE Power Electron. Spec. Conf.*, Jun. 2008, pp. 2191–2196.
[21] E. Romero-Cadaval, V. Minambres-Marcos, and M.-I. Milanes-Montero, "Analysis and optimization of sinusoidal voltage source inverter losses for variable output power applications," in *Proc. 7th Int. Conf.-Workshop Compat. Power Electron. (CPE)*, Jun. 2011, pp. 230–235.

JAIME PANDO-ACEDO received the B.S. degree in electrical engineering from the University of Extremadura, Badajoz, Spain, in 2015, where he is currently pursuing the Ph.D. degree. His current research interests include sensorless control of electrical drives, power electronics, and energy storage and management. He received a grant from the Junta de Extremadura in the Research Training Program, in 2017.

MARÍA ISABEL MILANÉS-MONTERO received the M.Sc. degree in industrial engineering and the Ph.D. degree in electrical and electronic engineering from the University of Extremadura, Spain, in 1997 and 2005, respectively. In November 1998, she joined the School of Industrial Engineering, University of Extremadura, as an Assistant Professor, and a Researcher with the Power Electrical and Electronic Systems Research and Development Group. Her major research interests include power quality, renewable energy sources control, energy storage management systems, smart grids, and electric vehicles.

ENRIQUE ROMERO-CADAVAL (Senior Member, IEEE) received the M.Sc. degree in industrial electronic engineering from the Escuela Técnica Superior de Ingeniería Industrial (ICAI), Universidad Pontificia de Comillas, Madrid, Spain, in 1992, and the Ph.D. degree from the Universidad de Extremadura, Badajoz, Spain, in 2004. In 1995, he joined the University of Extremadura, where he currently teaches power electronics and researches within the Power Electrical and Electronic Systems (PE&ES) Research and Development Group, School of Industrial Engineering. He is also a Coordinator of the Energy Group for the Intelligent Specialization (RIS3) of the Extremadura Region, Spain. His research interests include power electronics applied to power systems covering power quality, active power filters, electric vehicles, smart grids, and renewable energy resources. He is the Past President of the Power Electronics and Industrial Electronics Jointed Spanish Chapter, and the President of the Spanish Section of IEEE.

FERNANDO BRIZ (Senior Member, IEEE) received the M.S. and Ph.D. degrees from the University of Oviedo, Gijón, Spain, in 1990 and 1996, respectively. He is currently a Full Professor with the Department of Electrical, Computer and Systems Engineering, University of Oviedo. His research interests include electronic power converters and ac drives, power systems, machine monitoring and diagnostics, and digital signal processing. He is a member of the Steering Committee of IEEE Journal of Emerging and Selected Topics in Power Electronics (JESTPE). He received the IEEE Transactions on Industry Applications Award and nine IEEE Industry Applications Society Conference and the IEEE Energy Conversion Congress and Exposition Prize Paper Awards. He is the Past Chair of the Industrial Drives Committee of the Industrial Power Conversion System Department (IPCSD) of the IAS. He is the Vice Chair of IPCSD. He has served in scientific committees and as the Vice Chair or the Technical Program Chair for several conferences, including EECE, IEMDC, ICEM, ICEMS, and SLED. He is an Associate Editor of IAS and IEEE Journal of Emerging and Selected Topics in Power Electronics (JESTPE) Transactions.

FERMÍN BARRERO-GONZÁLEZ (Senior Member, IEEE) received the M.Sc. degree in electrical engineering from the Universidad Politécnica de Madrid, Madrid, Spain, in 1984, and the Ph.D. degree in electrical and electronic engineering from the Universidad Nacional de Educación a Distancia, Madrid, in 1995. He is currently a Professor of electrical engineering with the Universidad de Extremadura, Badajoz, Spain, where he is coordinating the Power Electrical and Electronic Systems Research Group. His research interests include power electronics in the power systems, flexible ac transmission systems, active power filters, and electrical machine drives.